Water-Mediated Network in the Resistance Mechanism of Fosfomycin

James McClory,[a] Jun-Tang Lin,[b] David Timson, [c] Jian Zhang [d] and Meilan Huang*[a]

Fosfomycin Resistance Kinase A (FomA) catalyzes the phosphorylation of fosfomycin, which is an effective antibiotic for treating urinary tract infections. Understanding the chemical reaction mechanism is essential for developing strategies to counter the resistance of fosfomycin in clinical settings. Here the catalytic mechanism of FomA was investigated using molecular dynamic simulations in conjunction with quantum mechanics/molecular mechanics calculations (B97d/AMBER99). Our QM/MM study disclosed that the phosphylation reaction catalyzed by FomA follows a dissociative mechanism, in contrast to previously proposed associative mechanism. In addition, we found that His58, a characteristic residue in the AAK family, plays a key role in positioning the phosphate group of fosfomycin in the transition state. Molecular dynamic simulations revealed the important roles of Lys9 and Lys18 in arranging the nucleotide for phosphate transfer. Furthermore, we identified a four-membered water network mediated by Asp171 and Ser13 that is critical in ordering ATP for phosphate transfer. The active structure and reaction mechanism of FomA will provide valuable insights for developing new strategies to tackle the resistance to Fosfomycin–based antibiotic therapies.

1 Introduction

Antimicrobial resistance is an emerging threat to the global public health as antibiotic-resistant strains of pathogenic bacteria are becoming increasingly prevalent.[1] Understanding the mechanism of antibiotic resistance would make it possible to design novel antibacterials or improve the current arsenal of antibacterials. Fosfomycin, an antibiotic effective for treating urinary tract infections (UTIs) discovered in 1969, is of particular interest due to its broad-spectrum activity against Gram-positive and Gram-negative pathogens.[2] However, lack of understanding on the drug-resistance mechanism of Fosfomycin has limited the development of novel or alternative antibiotic therapies to tackle its drug-resistance.

Fosfomycin (FM; CAS: 23155-02-4) is an inhibitor of the MurA enzyme,[3] which catalyses the first step of peptidoglycan synthesis. Fosfomycin is inactivated by Fosfomycin Resistance Kinase A (FomA) and Fosfomycin Resistance Kinase B (FomB) via two consecutive phosphate transfer reactions. FomA catalyses the Mg^{2+}-ATP dependant phosphate transfer to fosfomycin to produce the product Fosfomycin monophosphate (Figure 1), which is subsequently phosphorylated by FomB to yield fosofomyin diphosphate.[4]

FomA is a member of the amino acid kinase (AAK) family characterised by a three-layered αβα sandwich molecular architecture. The family is divided into two subdivisions; those which catalyse phosphate transfer to a phosphate group such as isopentenyl phosphate kinase (IPK),[5] uridine monophosphate kinase (UMPK)[6] and FomA,[7] and those which catalyse phosphate transfer to a carboxylate group such as carbamate kinase (CK),[8] aspartokinase (AK),[9] glutamate-5-kinase (G5K)[10] and N-acetyl-L-glutamate kinase (NAGK).[11] The conformational change of FomA induced upon substrate binding was investigated by a computational study.[12] However, so far, there is no report on phosphorylation reaction mechanism of FomA. Here we present the first theoretical study on the reaction mechanism of FomA by using molecular modelling, molecular dynamics and a combined QM/MM study and revealed that FomA actually catalyses the phosphorylation of fosfomycin through a dissociative reaction, instead of the previously suggested associative reaction mechanism.[7] Understanding the detailed reaction mechanism of FomA and the functions of the specific residues involved in phosphorylation would provide the theoretical basis for bypassing the inactivation of fosfomycin by FomA to tackle its antibiotic-resistance.

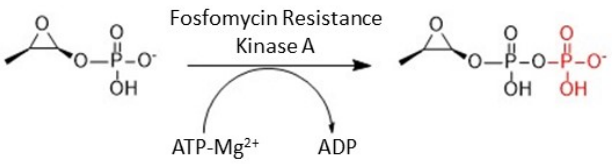

[a] School of Chemistry and Chemical Engineering, Queen's University Belfast, David Keir Building, Stranmillis Road, Belfast, BT9 5AG, Northern Ireland, United Kingdom
[b] Stem Cells and Biotheraphy Engineering Research Centre of Henan, College of Biomedical Engineering, Xinxiang Medical University, Xinxiang 453003, China
[c] School of Pharmacy and Biomolecular Sciences, The University of Brighton, Huxley Building, Lewes Road, Brighton, BN2 4GJ, United Kingdom
[d] Shanghai Jiaotong University, 280 Chongqing Road, Shanghai 200025, China
† Footnotes relating to the title and/or authors should appear here.
Electronic Supplementary Information (ESI) available: [details of any supplementary information available should be included here]. See DOI: 10.1039/x0xx00000x

Fig. 1 The FomA catalysed phosphorylation of fosfomycin to fosfomycin monophosphate mediated by ATP-Mg^{2+}

2 Theoretical Methods

2.1 Protein Preparation

FomA in complex with Mg^{2+}, ATP and the substrate was built by superimposing the ATP-Mg^{2+}-FomA complex (PDB Code: 3QUN) onto the crystal structure of ADP-$FMVO_3$-Mg^{2+}-FomA complex (PDB Code: 3QVF).[7] The vanadate group was removed from $FMVO_3$ to produce the ATP-FM-Mg^{2+}-FomA reactant complex. Protonation states were decided using ProPka[13] and by visual inspection.

2.2 Molecular Dynamics simulations

Molecular dynamics simulations were performed for the ATP-FM-Mg^{2+}-FomA complex using the GPU version of AMBER14[14] and and the FF14SB forcefield.[15] The parameters of ATP were obtained from the AMBER parameter database deposited by Bryce group[16] while RESP charges for the substrate were calculated through a single point charge calculation using Hartree-Fock (HF) theory and the 6-31g(d) basis set (Table S1) using Gaussian09.[17] The protein was solvated in an octahedral TIP3P water box composed of 7363 solvent molecules.Eleven sodium counter ions were used to neutralize the charge of the protein system. Electrostatic interactions were calculated using the particle mesh Ewald (PME) method[18] and a cutoff distance of 10 Å was used. The protein was subjected to two energy minimizations followed by 50 ps of equilibration using a NVT ensemble and Langevin dynamics with a force constant of 50 kcal $mol^{-1}A^{-2}$ to restrain the protein while it is heated slowly from 0 K to 300 K. 100ns production simulations were performed at 300 K in the NPT ensemble using Langevin dynamics and a time step of 2fs was used. SHAKE constraints[19] were applied to all bonds involving hydrogen atoms. Three replica MD simulations with random initial velocities were performed for each kinase complex system.

2.3 QM/MM Calculations

Cluster analysis was performed for the equilibrated trajectory of the MD simulations and a representative structure from cluster analysis with catalytically feasible configuration was selected for the subsequent QM/MM study. All QM/MM calculations were performed using the ONIOM method implemented in Gaussian09.[17] The QM layer was treated with the B97D functional to take into consideration Grimme's dispersion effect[20] and the 6-31g(d) basis set; the remainder of the molecular system was described at the molecular mechanics level using the Amber Parm99 force field[21]. The energies of the stationary points were calculated at the B97d/6-311++g(2df) level of theory (Table S2). An electronic embedding scheme was implemented to incorporate the partial charges of the MM region into the quantum mechanical Hamiltonian[22]. QM/MM was set up according to the Tao protocol[23] where the residues within 6 Å of the active site of the ATP-FM-Mg^{2+}-FomA complex were allowed to move freely while the remainder of the system was frozen.

The QM region was composed of the triphosphoryl side chain and truncated methyl group of ATP, the substrate fosfomycin, Mg^{2+} and three coordinating water molecules. Lys9, Lys18, Lys216, His58, Asp208 and Asp150 were also included in the QM region with their side chains truncated. In total 42 heavy atoms were included in the QM region. Hydrogen link atoms were utilized to cap the bonds crossing into the MM region.[24-25]

RESP charges used for ATP and fosfomycin in the MD simulations were implemented in the QM/MM calculations. The initial structures obtained from cluster analysis of the MD trajectory were subjected to a geometric optimization and then used as the starting structure for a potential energy scan. The reaction coordinate was set as the distance between the γ-phosphate phosphorous of ATP and the protonated phosphate oxygen of the substrate Fosfomycin, and scanned in an increment of 0.1 Å. The structure taken from the saddle point of the PES scan was optimized as a transition state and validated by the characteristic unique imaginary frequency. An IRC calculation was used to link the stationary points along the reaction pathway.

3 Results and Discussion

3.1 Catalytically competent structure of ATP-FM-Mg^{2+}-FomA complex

In the crystal structure of *Streptomyces wedmorensis* FomA in complex with fosfomycin and MgAMPPNP, the distance between the oxygen atom of fosfomycin phosphate and phosphorus atom of AMPPNP (5.2 Å) is too far for the in-line phosphate transfer to happen (Figure 2a).[26] Further, several crystal structures of FomA complexed with ATP and fosfomycin were reported,[7] among which, only the ADP-$FMVO_3$-Mg^{2+}-FomA complex (PDB Code: 3QVF) contained an ordered catalytic site. In order to attain an catalytically competent ATP-FM-Mg^{2+}-FomA complex so as to investigate the mechanism of the phosphate-transfer reaction catalyzed by FomA, we built a complete FomA complex model by superimposing ADP-$FMVO_3$-Mg^{2+}-FomA and ATP-Mg^{2+}-FomA complex (PDB Code: 3QUN).

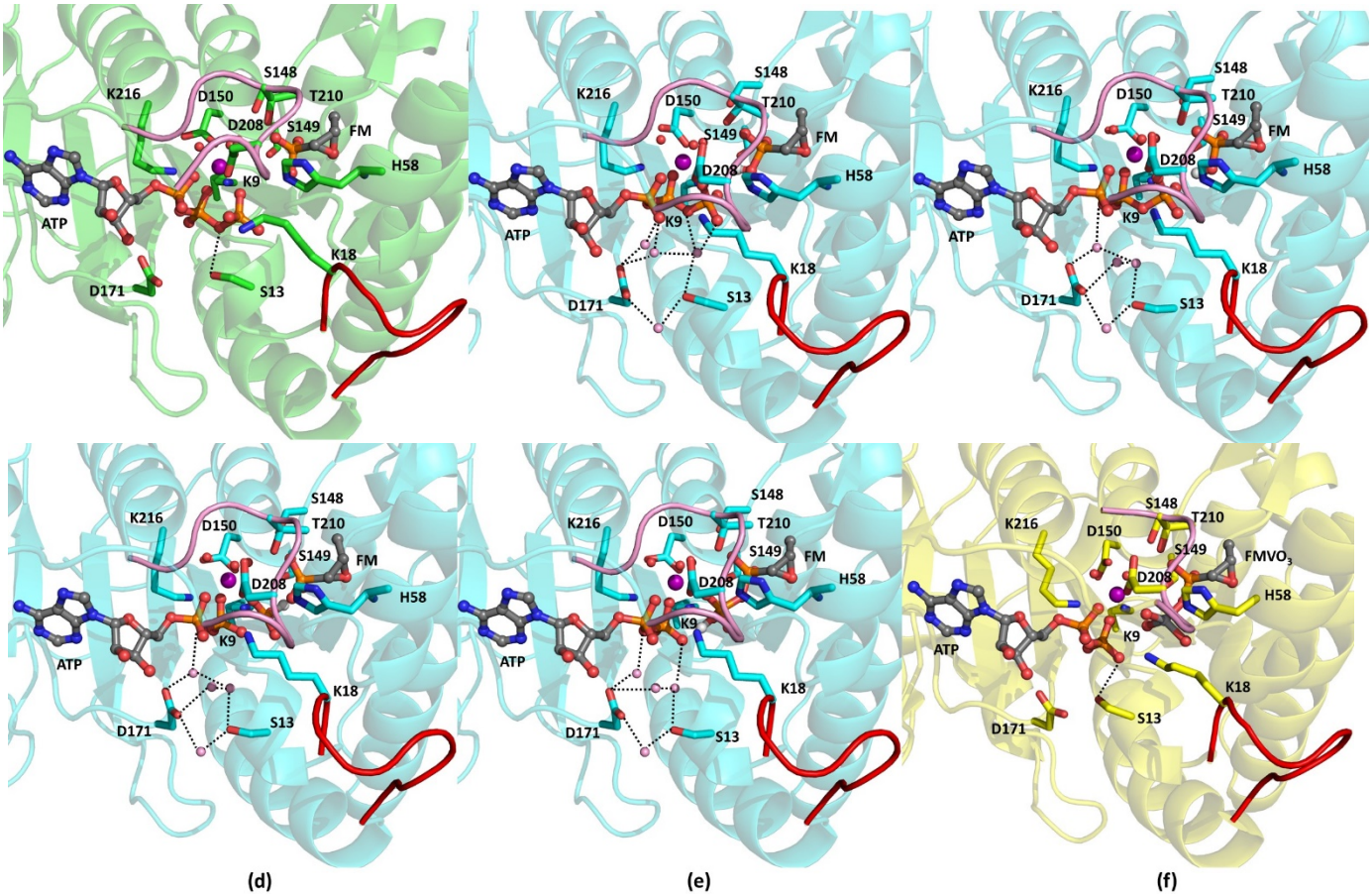

Fig. 2 Representative structures from different stages of the FomA reaction mechanism (a) Crystal structure of *Streptomyces wedmorensis* FomA in complex with AMPPNP, Mg2+ and Fosfomycin (PDB Code: 3D41) (b) representative structure from cluster analysis of MD trajectory (c) QM/MM optimised reactant structure (d) QM/MM optimised transition state structure (e) QM/MM optimised product structure (f) Crystal structure of *Streptomyces wedmorensis* FomA in complex with ADP, Mg2+ and FMVO3 (PDB Code: 3QVF). The glycine-rich loop consisting residues 16-24 is shown in red.

The γ-phosphate of ATP in the resulting complex model was located 4.4 Å from the phosphate group of fosfomycin and favourably orientated for in-line phosphate transfer (Figure S1), representing a catalytically competent pose of the nucleotide. Root mean square deviation (RMSD) values of the protein Cα atoms were calculated with the initial structure as the reference structure. This showed that the system equilibrated after 10 ns (Figure S3). In the ATP-FM-Mg^{2+}-FomA reactant model (Figure S3), the distance between the γ-phosphate of ATP and the phosphate group of fosfomycin was 4.4 Å.

Since the pose of ATP in the reactant ATP-FM-Mg^{2+}-FomA complex model was taken from the nucleotide in the crystal structure of ATP-Mg^{2+}-FomA (PDB Code: 3QUN), it was necessary to examine the conformational stability of the nucleotide in the built model during MD simulations. RMSD analysis was performed on ATP using the initial ATP pose as a reference. From the RMSD plot of the heavy atoms in ATP (Figure S3), it can be seen that the average RMSD value was approximately 0.5 Å, indicating the nucleotide was evolved into a stable conformation. With time evolution, ATP adopted a favourable orientation to facilitate phosphate transfer with the distance between the γ-phosphate of ATP and the phosphate group of fosfomycin being 3.4 Å (Figure S4). Superimposition of ATP from the MD representative structure and that in the original complex model revealed significant changes in the triphosphoryl moiety of ATP (Figure S1), which may be indispensable for reorganizing of the catalytic site of FomA during phosphate transfer.

In the crystal structures of FomA,[7,26] His58 does not directly form a hydrogen bond with the γ-phosphate group of ATP/AMPPNP and the substrate phosphate, although it is in the proximity of both the substrate phosphate and the γ-phosphate of ATP. Instead, it is tethered by a structural water molecule around the vicinity of the substrate and the nucleotide. Interestingly, with time evolution of the MD simulations, His58 moves closer to the catalytic centre, forming hydrogen bonds with both substrate phosphate and the γ-phosphate of ATP and thus rigidifying/ordering the flexible phosphate tail of ATP in the catalytic site (Table S3). The entropy loss associated with rigidification of ATP may be compensated by additional interactions with the surrounding residues.

An ordered Lysine triangle composed of Lys9, Lys18 and Lys216 (Figure S2) in AAK kinases has been suggested to be crucial for the catalytic reaction. Structural and mutagenesis studies of FomA together with sequence comparison with its homologous enzymes

indicated Lys9 and Lys216 participate the interaction with the phosphate tail of ATP, while Lys18 stabilizes transition state.[7] In the crystal structure of FomA in complex with ATP or AMPPNP,[7,26] Lys9 interacts with the β-phosphate of ATP or AMPPNP. Interestingly, our MD simulations show that Lys9 formed favourable interactions with both β- and γ-phosphate of ATP with the movement of the flexible ATP tail (Figure 2b). In the crystal structure of FomA, Lys18 on the glycine rich loop is in the proximity of the γ-phosphate of ATP and Asp208, which is located on the flexible loop connecting α-helix 6 and α7. Notably, with time evolution of the MD simulations, while Lys18 remained in the salt-bridge interaction with Asp208, it approaches the α-phosphate, forming ionic interactions with both α- and γ-phosphate, and thus greatly restraining the flexibility of the tri-phosphate tail of ATP (Figure 2b, Figure S4).

Furthermore, our MD simulations showed Asp208 remains hydrogen bonded with a coordinating water, as observed in the crystal structure of FomA.[26] Thus Asp208 not only organizes the Mg^{2+} coordination via the hydrogen bond interaction with a coordinating water, but also helps to reorganize the catalytic pocket via the ionic interaction with Lys18, which in turn orders the flexible phosphate tail of ATP, facilitating the phosphate transfer.

3.2 QM/MM calculations revealed a dissociative transition state of FomA

The crystal structure of the ADP-$FMVO_3$-Mg^{2+}-FomA complex was resolved with a vandate ion used to mimic the γ-phosphate of ATP in order to mimic the transition state.[7] However, the bond lengths corresponding to the reaction coordinates in the complex indicate that it is more analogous to the product complex than the postulated transition state structure. Therefore, ambiguity still surrounds the actual reaction mechanism of FomA.

To acquire a comprehensive understanding of the reaction mechanism of FomA, the chemical reaction pathway concerning phosphate transfer was studied using QM/MM. Cluster analysis was performed on the last 10 ns of the 100 ns MD simulation and a representative structure for further QM/MM calculations was chosen based on the occurrence and liability for a phosphoryl reaction to occur. Starting from the representative structure resulting from the MD simulations of the ATP-FM-Mg^{2+}-FomA complex, QM/MM calculations were performed using the QM/MM (B97d/6-31G(d):AMBER99), whereby the QM calculation was performed at the B97d/6-31G(d) theory level, and the MM calculation was carried out using the AMBER99 force field. The B97d functional was chose since it was found to perform well on fellow AAK, IPK[27].

The QM/MM optimized structures of the reactant, TS and product show that Lys18 remains in ionic interactions with Asp208 and the α- and γ–phosphate of ATP, helping to position the nucleotide and organize the catalytic site during phosphate transfer (Figure 2c-e). During phosphate transfer, negative charge would accumulate upon the cleavage of the bond between the β- and γ-phosphate of ATP. In the QM/MM optimized stationary point structures of FomA, Lys18 remains in the close proximity of the β-, γ-bridging oxygen, stabilizing the negative charge developed during phosphate transfer.

A previous site directed mutagenesis study implicated His58 in stabilising the transition state.[7] The corresponding histidine residue His50 in IPK, another kinase in the 'phosphate' subdivision of the AAK family, was also suggested to be crucial for substrate binding and stabilizing the transition state (TS) from previous mutagenesis studies and a QM/MM study.[27,28] In our QM/MM optimized structures of the reactant, transition state and product, His58 remained tethered between the substrate phosphate and the γ-phosphate of ATP (Figure 2). Thus our results show that His58 plays a predominant role in positioning the substrate in the catalytic site and stabilizing the transition state during phosphate transfer. This is in good accordance with previous mutagenesis studies on FomA[7] as well as the kinetic and QM/MM studies on its homologous kinase IPK.[27,28]

QM/MM studies on IPK[27] revealed that the backbone amide of Gly8 stabilized the TS by forming a hydrogen bond with the β-, γ-bridging oxygen atom of ATP. In the optimized TS structure of FomA, the corresponding glycine residue Gly12 on a γ-turn secondary structure also forms a hydrogen bond with the β-, γ-bridging oxygen of ATP (Figure S5), indicating Gly12 also participates the stabilization of the TS of FomA.

Enzyme kinetic analysis of the conversion of fosfomycin catalyzed by *Streptomyces wedmorensis* FomA-revealed a turnover number (k_{cat}) of 155.9 s^{-1}, which corresponds to a free energy barrier of 14.46 kcal mol^{-1}.[7] The estimated energy barrier from QM/MM calculations is 17.31 kcal mol^{-1} (Figure 3). Thus, the calculated energy barrier is in good agreement with the previously measured experimentally determined kinetic constant.

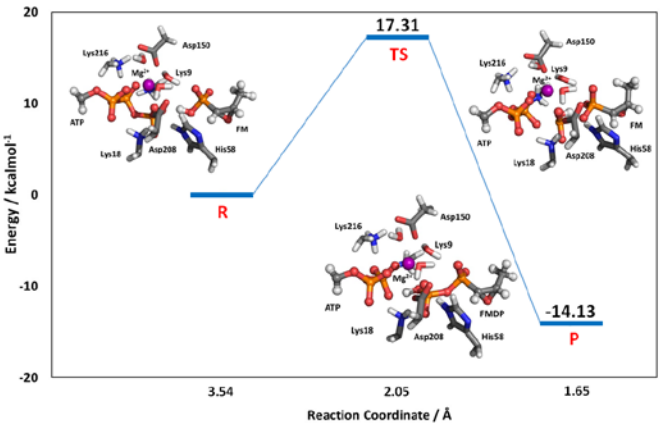

(a)

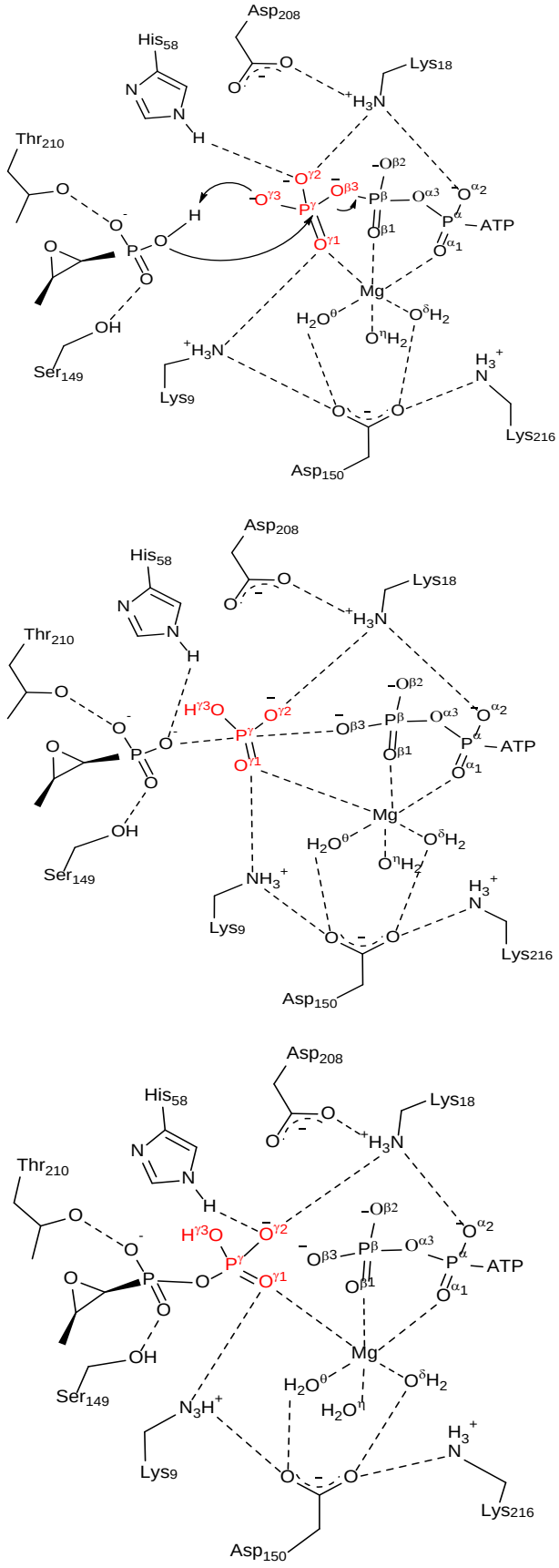

Fig. 3 (A) QM/MM energy profile for the phosphorylation of fosfomycin. (B) 2-D sketch of phosphate transfer in FomA. The reaction coordinates correspond to the distance between the phosphate oxygen of fosfomycin and the γ-phosphate of ATP, and the distance between the P^{γ} of ATP and $O^{\beta 3}$.

An associative reaction mechanism was proposed for FomA based on the crystal structures of FomA.[7] The associative or dissociative character of the transition state can be estimated using Pauling's formula: $D(n) = D(1) - 0.6 \log n$.[29] Here, $D(1) = 1.73$ Å representing the average length of a P–O bond, and $D(n)$ is defined as the average of the two P–O distances (2.05 Å) in the transition state structure. The estimated fractional bond number (n) associated with the QM/MM optimized geometry of the transition state is 0.30, indicated a dissociative character of 70%. This is similar to IPK, another AAK kinase, for which a dissociative nature of the TS was also proposed.[27]. Thus our calculations revealed that the phosphorylation catalysed by FomA proceeds with a dissociative mechanism (Figure 4), instead of the previously proposed associative mechanism.

In cyclin-dependent (protein) Kinase-2 (CDK2), Mg^{2+} is also coordinated to α-, β-, γ- phosphates of ATP. However, in contrast to the reaction catalyzed by CDK2, which is assisted by a general base,[30] Asp208, although close to the titratablecatalytic residue His58, does not function as a catalytic base in FomA. In the present research, we determined that the reaction catalyzed by FomA occurs via a direct phosphorylation mechanism (Figure 3), similar to that found for two GHMP kinases, galactokinase (GALK) and PMK[31,32] as well as another AAK kinase IPK.[27]

3.3 Water-assisted network in ordering the nucleotide in the active site of FomA

In the crystal structures of ADP-$FMVO_3$-Mg^{2+}-FomA (PDB code: 3QVF)[7] and AMPPNP-FM-Mg^{2+}-FomA (PDB code: 3D41),[26] Ser13 forms a hydrogen bond with the oxygen or nitrogen atom corresponding to the β-, γ-bridging oxygen atom of ATP (Figure 2f). In the crystal structure of FomA complexed with ATP and fosfomycin (PDB code: 3QUO), Ser13 is hydrogen bonded to β-phosphate. Interestingly, from our MD simulations, we found Ser13 is tethered in the catalytic site by a hydrogen bond network mediated by four structural water molecules (Table S3). One of these water molecules is hydrogen bonded to Ser13, the γ–phosphate and a second water molecule, which is in turn hydrogen bonded to Asp171 and the α-phosphate oxygen (Figure 2b, Figure 4). Another water molecule tethers Asp171 and the α-phosphate of ATP by additional hydrogen bonds. This water-mediated hydrogen bond network breaks up following the approach of Lys18, which functions to order and rigidify the ATP triphosphate tail. A fourth water nestles between Asp171 and Ser13. In the QM/MM optimized reactant and TS structures (Figure 2c, 2d, 2e), such four-water hydrogen bond network is generally maintained. However, it should be noted that the water linking Ser13 and γ-phosphate moves further away from γ-phosphate so that it allows the γ-phosphate to be transferred. Interestingly, in the QM/MM optimized product, the tight four

water network as observed in the MD simulated complex structure is resumed, with a water linking Ser13 and β-phosphate of ATP. Thus the water-mediated hydrogen bond network in the catalytic site of FomA is important in ordering the ATP nucleotide, facilitating the phosphate transfer.

Water is essential for cell and molecular biology, and so water-mediated networks may play a significant role in the function of kinases, and therefore novel kinase inhibitors may be developed by interfering with the structural water in the catalytic site.[33] For example, Aurora kinase A was found to be activated by the spindle-associated protein mediated by a water network.[34] A clinical kinase inhibitor Bosutinib displays its selectivity by engaging the conserved water-mediated hydrogen bond network in the active site.[35] The well maintained, water-assisted hydrogen bond network in FomA identified in the present work would be useful for design of novel selective drug therapies to tackle the drug resistance to fosfomycin.

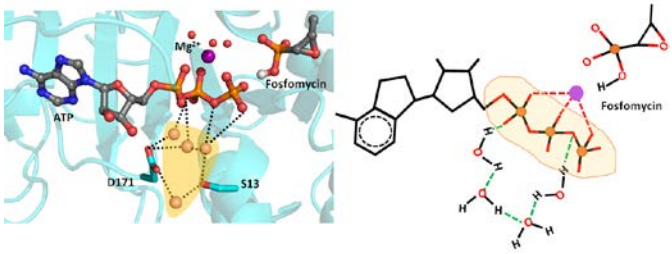

Fig. 4 Water mediated hydrogen bond network around the phosphate tail of ATP in the active site of FomA.

3.4 The role of the key residues revealed by MD simulations of the mutants

The key residues of FomA were mutated and MD simulations were performed on these mutants to understand their role in the activity of the kinase and the binding of substrates.

H58A/L

Both FomA and IPK belong to AAK kinase family. In *Methanocaldococcus jannaschii* IPK, mutating His60 (corresponding to His58 in FomA) to alanine or asparagine resulted in no detectable activity while the H60Q mutation resulted in significantly reduced catalytic efficiency.[28] Similarly, mutation of His58 in FomA resulted in no detectable activity in the enzyme.[7] Recently, a QM/MM study of *Thermoplasma acidophilum* IPK suggested that His50 (corresponding to His58 in FomA) plays an important role in substrate binding.[27] In the WT FomA, Lys18 is located between the α- and γ-phosphate groups of ATP, assisting in positioning the nucleotide for phosphate transfer (Figure 2B-2D), whereas in simulated structure of the H58A mutant, Lys18 moves away from the α- phosphate and is located between γ-phosphate groups of ATP and the substrate phosphate group (Figure 5A), and therefore the resulting configuration is unfavourable for substrate binding and stabilizing the TS. In addition, the ionic interaction between Lys18 and Asp208 observed in the WT enzyme is abolished in the H58A variant. Thr210, which is hydrogen bonded to a coordinating water in the WT kinase, is found to form a hydrogen bond with Asp208 in the variant. In comparison with the WT kinase, the phosphate tail of nucleotide in the H58A mutant is largely flexible, which is mainly due to the significant conformational change around the flexible loop connecting α-helix 6 and α7 (where Asp208 and Thr210 are located) (Figure S6).

Remarkably, due to the absence of the histidine side chain at the γ-phosphate of ATP, Ser13 turned towards the γ-phosphate group of the nucleotide. As a result, the water network observed in the WT kinase is disrupted and Asp171 moves away from the active site, such that the water–mediated network around ATP observed in the WT kinase is lost in the mutant. In the MD simulated structure of WT kinase, Ser148 forms a hydrogen bond with the phosphate group of fosfomycin substrate, whereas in the H58A mutant the hydrogen bond is disrupted, such that the substrate cannot be positioned appropriately anymore.

MD simulation of H58L was also conducted. It was found that in the variant Lys216 turns toward Thr170 to establish a hydrogen bond, so that the ionic interaction between Lys216 and Asp150 observed in the WT kinase is diminished (Figure S7A).

S13A and D171A

In the D171A mutant, the distance between the phosphate group of the substrate fosfomycin and γ-phosphate of ATP in the MD simulated structure is increased to 4.0 Å (from 3.4Å in the WT kinase), making the reaction less favourable. Due to the D171A mutation, the ionic interaction between Asp171 and Ser13 observed in the WT kinase is lost. As a result, Ser13 approaches the γ-phosphate of ATP and the four-membered water network observed in the WT MD simulation is changed into a two-water network (Figure 5B). In the S13A mutant, Asp171 pointed away from active site due to lack of the ionic interaction with Ser13 so that the water-network that assists organizing ATP in the catalytic site is also reduced (Figure S7B).

K9A, K18A and K216A

Kinetic studies showed a ~40 fold decrease in k_{cat} for the K9A mutation compared to the WT enzyme.[7] The MD simulated structure of K9A shows that Asp171 moves away from Ser13, and that Ser13 directly bonds to the γ-phosphate of ATP (Figure 5C). The loop where Asp208 and Thr210 are located also undergoes significant changes and the substrate is pushed away from the ATP γ-phosphate so that Thr210 no longer binds the phosphate group of the substrate. The four-water network observed in the WT kinase is reduced to a one-water network.

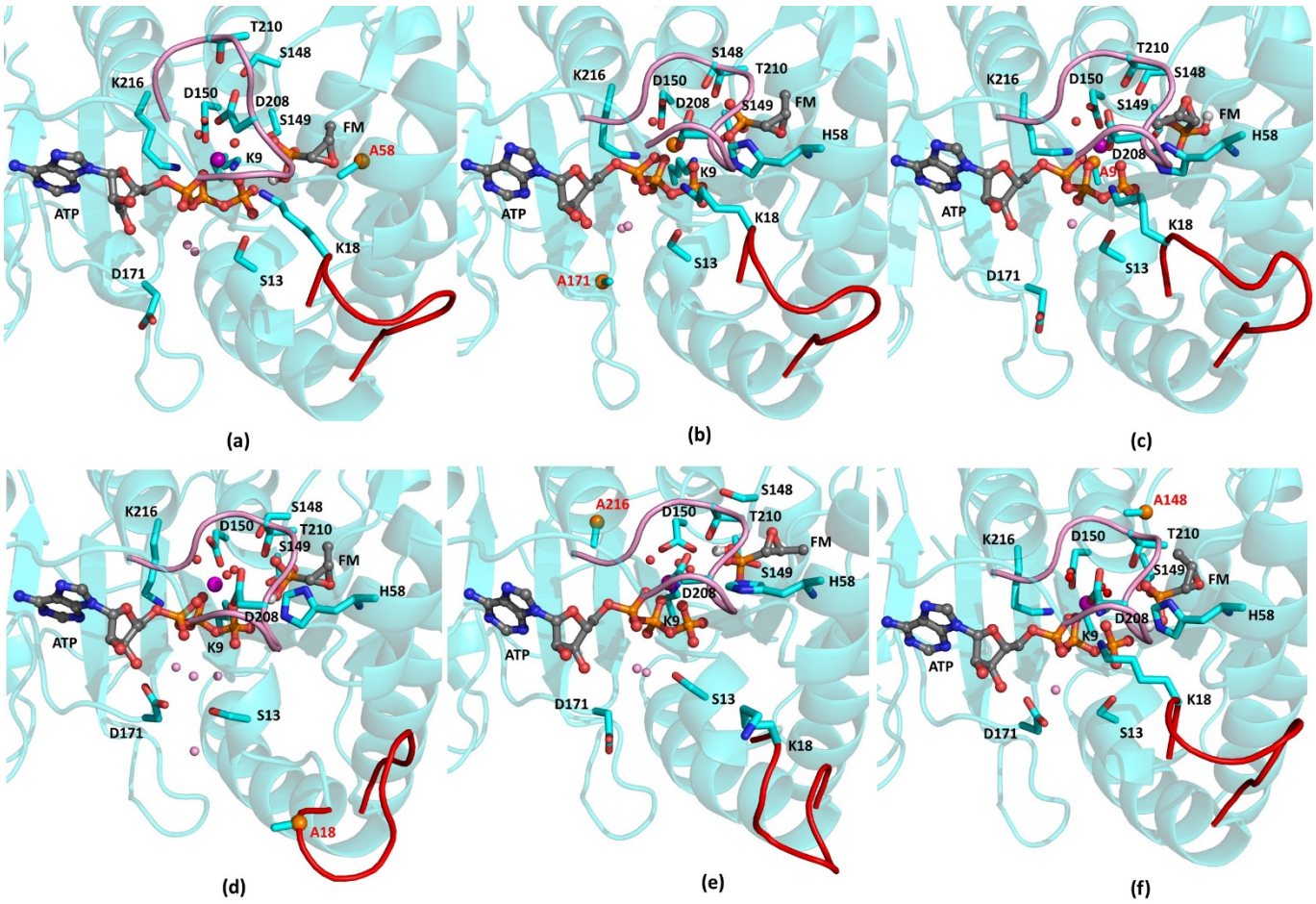

Fig. 5 Representative structures of FomA mutants from MD simulations (a) H58A (b) D171A (c) K9A (d) K18A (e) K216A (f) S148A. The glycine-rich loop is shown in pink and the loop connecting α-helix 6 and α-helix 7 is shown in red.

FomA exhibited no detectable activity when Lys18 was mutated into alanine.[7] From our simulation, significant conformational changes around the glycine-rich loop were observed in both K18A and K216A (Figure 5D&5E, Figure S6). In the K216A mutant, Lys18 moves away from the active site such that ATP and the substrate are no longer in a favourable distance or orientation to each other for the phosphate transfer to occur (Figure 5E). In addition, His58 moves away from ATP and is only hydrogen bonded with the substrate fosfomycin. In addition, Ser13 approaches the γ-phosphate of ATP and Asp171 turns away from the active centre due to loss of the ionic interaction with Ser13, such that four-water network in the WT kinase changes into a two-water network.

S148A and S149A

Kinetic data showed that two tandem serine residues, Ser148 and Ser149, are critical for substrate binding and FomA's activity. S148A mutation caused a ~4-fold decrease in k_{cat} and a ~17-fold increase in $K_M$for fosfomycin. A S149A mutation led to a ~10-fold decrease in activity and a 39-fold increase in K_M for fosfomycin.[7] Our MD simulations of the S148A mutant show the Ser13 turns towards the γ-phosphate of ATP, and the ionic bond with Asp171 is broken. As a result the water network rigidifying ATP is disrupted (Figure 5F). MD simulations of the S149A mutation show both Asp171 and Ser13 move away from the active site and Ser13 forms a hydrogen bond interaction with the γ-phosphate of ATP, such that the four-water network in the WT kinase is reduced to two-water network (Figure S7E).

D208A, D150A and T210A

Kinetic studies showed that the D208A mutation caused a ~13-fold decrease in k_{cat}.[7] MD simulations of D208A show the loop where the aspartate is located experienced notable conformational change (Figure S7C). Thr215, which is hydrogen bonded to the backbone oxygen of Thr210 on the loop in the WT kinase, becomes surface exposed in the variant.

In the WT FomA, Asp150 forms an ionic interaction with Lys216. MD simulations of the D150A mutant show that due to the loss of ionic interaction with Asp150, Lys216 turns toward Thr170, establishing a new hydrogen bond. The loop where Asp208 and Thr210 are located exhibits remarkable conformational change (Figure S7D), such that the hydrogen bond between Thr210 and Thr215 present in the WT kinase is lost in the D150A variant. In addition, Ser13 moves away from the active site resulting in an attenuated water network. Thus

Asp150 may play a predominant role in organizing the active site of FomA via the loop surrounding phosphate tail of the ATP.

A mutagenesis study showed that a T210A mutation led to no detectable activity or binding affinity of fosfomycin.[7] In our MD simulations of T210A (Figure S7F), the substrate moved away from the nucleotide ATP due to the loss of the hydroxyl moiety of Thr210, which forms a hydrogen bond with fosfomycin in the WT kinase. His58 moves away from the substrate fosfomycin and is only hydrogen bonded with the γ-phosphate of ATP. Furthermore, Ser13 and Asp171, which mediate the water network around ATP in the WT kinase, turns away from the catalytic site and Ser13 becomes directly hydrogen bonded to the γ-phosphate of ATP.

Conclusions

Understanding the drug resistance mechanism of fosfomycin is a critical task in tackling the ongoing problem of antibiotic resistance. Previously crystallography studies revealed different states of FomA during the phosphate transfer process, however, the complete complex structure representing a catalytically competent conformation and transition state structure have not been elucidated, resulting in ambiguity remaining around the reaction mechanism. Therefore, it was necessary to elucidate the catalytically active conformation of the kinase and the reaction mechanism in order to tackle the challenge of antibiotic resistance of fosfomycin.

Here, based on MD simulations on the ATP-FM-Mg^{2+}-FomA reactant complex, we found that Lys18 plays a pivotal role in positioning the nucleotide to facilitate the phosphate transfer. Further we identified a water network mediated by Asp171 and Ser13 which is crucial in maintaining ATP in a catalytically competent conformation. MD simulations on the mutants generated by mutating His58, Thr210, two tandem serine Ser148/Ser149and the lysine triad comprising Lys9, Lys18 and Lys216 disclosed that these residues play significant role in the water network identified involving Asp171 and Ser13, further underpinning the importance of the water-mediated network in maintaining an ordered nucleotide in the active site of FomA.

A QM/MM study was performed to study the reaction mechanism of FomA and a dissociative reaction mechanism was revealed, which is analogous to the homologous AAK kinase IPK, but in contrast to the previously proposed associative mechanism for FomA. The QM/MM study further revealed that His58 plays a significant role in substrate binding as proposed in the previous literature[7] where it was suggested to position the ATP molecule in the transition state. The water-mediated network in the catalytic centre of FomA and the elucidated drug resistance mechanism of fosfomycin in the present study would provide valuable insights for development of novel or alternative therapies to tackle the antibiotic-resistance of fosfomycin. Potential strategies include developing fosfomycin analogues inhibit that disrupt the four-water network or which are not compatible with binding to four-water-FomA; de novo design of novel compounds that disrupt the four-water network in FomA; alternatively; developing TS analogues to inhibit FomA directly, based on the mechanism revealed in the present study.

Conflicts of interest

There are no conflicts to declare

Acknowledgements

J.M. acknowledges the financial support from the Department of Education and Learning (DEL), Northern Ireland. We are grateful for the computing resources from QUB high performance computing centre.

References

1 L. L. Silver, *Clin Microbiol Rev*, 2011, **24**, 71–109.
2 K. L. Fillgrove, S. Pakhomova, M. E. Newcomer and R. N. Armstrong, *J. Am. Chem. Soc.*, 2003, **125**, 15730–15731.
3 F. M. Kahan, J. S. Kahan, P. J. Cassidy and H. Kropp, *Ann. N. Y. Acad. Sci.*, 1974, **235**, 364–386.
4 S. Kobayashi, T. Kuzuyama and H. Seto, *Antimicrob Agents Chemother*, 2000, **44**, 647–650.
5 M. F. Mabanglo, H. L. Schubert, M. Chen, C. P. Hill and C. D. Poulter, *ACS Chem. Biol.*, 2010, **5**, 517–527.
6 C. Marco-Marín, F. Gil-Ortiz and V. Rubio, *J. Mol. Biol.*, 2005, **352**, 438–454.
7 S. Pakhomova, S. G. Bartlett, P. A. Doerner and M. E. Newcomer, *Biochemistry*, 2011, **50**, 6909–6919.
8 A. Marina, P. M. Alzari, J. Bravo, M. Uriarte, B. Barcelona, I. Fita and V. Rubio, *Protein Sci.*, 1999, **8**, 934–940.
9 C. Marco-Marín, S. Ramón-Maiques, S. Tavárez and V. Rubio, *J. Mol. Biol.*, 2003, **334**, 459–476.
10 C. Marco-Marín, F. Gil-Ortiz, I. Pérez-Arellano, J. Cervera, I. Fita and V. Rubio, *J. Mol. Biol.*, 2007, **367**, 1431–1446.
11 S. Ramón-Maiques, A. Marina, F. Gil-Ortiz, I. Fita and V. Rubio, *Structure*, 2002, **10**, 329–342.
12 Y.-J. Wu, Q.-C. Zheng, J.-L. Zhang, W.-T. Chu, Y.-L. Cui, Y. Wang and H.-X. Zhang, *J Mol Model*, 2014, **20**, 2236.
13 M. H. M. Olsson, C. R. Søndergaard, M. Rostkowski and J. H. Jensen, *J Chem Theory Comput*, 2011, **7**, 525–537.
14 D. A. Case, V. Babin, J. T. Berryman, R. M. Betz, Q. Cai, D. S. Cerutti, T. E. Cheatham III, T. A. Darden, R. E. Duke, H. Gohlke, A. W. Goetz, S. Gusarov, N. Homeyer, P. Janowski, J. Kaus, I. Kolossváry, A. Kovalenko, T. S. Lee, S. LeGrand, T. Luchko, R. Luo, B. Madej, K. M. Merz, F. Paesani, D. R. Roe, A. Roitberg, C. Sagui, R. SalomonFerrer, G. Seabra, C. L. Simmerling, W. Smith, J. Swails, R. C. Walker, J. Wang, R. M. Wolf, X. Wu and P. A. Kollman, *AMBER 14*, University of California, San Francisco, 2014.
15 J. A. Maier, C. Martinez, K. Kasavajhala, L. Wickstrom, K. E. Hauser and C. Simmerling, J. *Chem. Theory Comput.*, 2015, **11**, 3696–3713.
16 K. L. Meagher, L. T. Redman and H. A. Carlson, *J Comput Chem*, 2003, **24**, 1016–1025.
17 M. J. Frisch, G. W. Trucks, H. B. Schlegel, G. E. Scuseria, M. A. Robb, J. R. Cheeseman, G. Scalmani, V. Barone, B. Mennucci, G. A. Petersson, H. Nakatsuji, M. Caricato, X. Li, H. P. Hratchian, A. F. Izmaylov, J. Bloino, G. Zheng, J. L. Sonnenberg, M. Hada, M. Ehara, K. Toyota, R. Fukuda, J. Hasegawa, M.

Ishida, T. Nakajima, Y. Honda, O. Kitao, H. Nakai, T. Vreven, J. A. Montgomery, Jr., J. E. Peralta, F. Ogliaro, M. Bearpark, J. J. Heyd, E. Brothers, K. N. Kudin, V. N. Staroverov, R. Kobayashi, J. Normand, K. Raghavachari, A. Rendell, J. C. Burant, S. S. Iyengar, J. Tomasi, M. Cossi, N. Rega, J. M. Millam, M. Klene, J. E. Knox, J. B. Cross, V. Bakken, C. Adamo, J. Jaramillo, R. Gomperts, R. E. Stratmann, O. Yazyev, A. J. Austin, R. Cammi, C. Pomelli, J. W. Ochterski, R. L. Martin, K. Morokuma, V. G. Zakrzewski, G. A. Voth, P. Salvador, J. J. Dannenberg, S. Dapprich, A. D. Daniels, Ö. Farkas, J. B. Foresman, J. V. Ortiz, J. Cioslowski, and D. J. Fox, *Gaussian 09, Revision D.01*, Gaussian, Inc., Wallingford CT, 2009.

18 T. Darden, D. York and L. Pedersen, *The Journal of Chemical Physics*, 1993, **98**, 10089–10092.

19 J. Ryckaert, G. Ciccotti and H. J. C. Berendsen, *J. Comput. Phys*, 1977, 327–341.

20 S. Grimme, *J Comput Chem*, 2006, **27**, 1787–1799.

21 T. E. Cheatham, P. Cieplak and P. A. Kollman, *J. Biomol. Struct. Dyn.*, 1999, **16**, 845–862.

22 T. Vreven, K. S. Byun, I. Komáromi, S. Dapprich, J. A. Montgomery, K. Morokuma and M. J. Frisch, *J. Chem. Theory Comput.*, 2006, **2**, 815–826.

23 P. Tao and H. B. Schlegel, *J. Comput. Chem.*, 2010, **31**, 2363–2369.

24 A. Warshel and M. Levitt, *J. Mol. Biol.*, 1976, **103**, 227–249.

25 U. C. Singh and P. A. Kollman, *J. Comput. Chem.*, 1986, **7**, 718–730.

26 S. Pakhomova, S. G. Bartlett, A. Augustus, T. Kuzuyama and M. E. Newcomer, *J Biol Chem*, 2008, **283**, 28518–28526.

27 J. McClory, D. J. Timson, W. Singh, J. Zhang and M. Huang, *J Phys Chem B*, 2017, **121**, 11062–11071. T

28 N. Dellas and J. P. Noel, *ACS Chem. Biol.*, 2010, **5**, 589–601.

29 A. S. Mildvan, *Proteins*, 1997, **29**, 401–416.

30 G. K. Smith, Z. Ke, H. Guo and A. C. Hengge, *J. Phys. Chem. B*, 2011, **115**, 13713–13722.

31 M. Huang, X. Li, J.-W. Zou and D. J. Timson, *Biochemistry*, 2013, **52**, 4858–4868.

32 M. Huang, K. Wei, X. Li, J. McClory, G. Hu, J.-W. Zou and D. Timson, *J. Phys. Chem. B*, 2016, **120**, 10714–10722.

33 P. Ball, *Proc. Natl. Acad. Sci*. USA, 2017, 201703781.

34 S. Cyphers, E. F. Ruff, J. M. Behr, J. D. Chodera and N. M. Levinson, *Nat. Chem. Biol.*, 2017, **13**, 402–408.

35 N. M. Levinson and S. G. Boxer, *Nat. Chem. Biol.*, 2014, **10**, 127–132.